coatings

MDPI

Article

Tribological Behavior of Structural Steel with Different Surface Finishing and Treatments for a Novel Seismic Damper

Eleonora Grossi [1,*], Enrico Baroni [2], Alessandra Aprile [1], Annalisa Fortini [2], Matteo Zerbin [1] and Mattia Merlin [2]

[1] Structural Engineering Group, Department of Engineering, University of Ferrara, 44122 Ferrara, Italy
[2] Metallurgy Group, Department of Engineering, University of Ferrara, 44122 Ferrara, Italy
* Correspondence: eleonora.grossi@unife.it

Abstract: In the context of developing an innovative seismic dissipation system, which aims to compromise on the steadiness of friction and processes costs, this work deals with the tribological characterization of an S355JR structural steel, whose surface has been preliminarily treated by different mechanical and galvanic processes. Tribological tests were performed in a pin-on-disk configuration and in reciprocating motion, using values of 1 Hz and 2 Hz as the motion inversion frequency, a constant normal load of 50 N, and variable test duration, according to the most frequent seismic events. The tribological system was composed of S355JR structural steel pins and disks of the same steel, which were alternatively treated by electrolytic nickel plating, electrolytic zinc plating, and two different shot peening processes. The results highlight that while electrolytic nickel increments the overall steadiness of the coefficient of friction (COF), electrolytic zinc plating guarantees the longest first steady-state stage and a COF lower than the one guaranteed by the coupling of untreated pins and disk.

Keywords: steel; wear; pin-on-disk; nickel plating; zinc plating; shot peening

Citation: Grossi, E.; Baroni, E.; Aprile, A.; Fortini, A.; Zerbin, M.; Merlin, M. Tribological Behavior of Structural Steel with Different Surface Finishing and Treatments for a Novel Seismic Damper. *Coatings* **2023**, *13*, 135. https://doi.org/10.3390/coatings13010135

Academic Editor: Csaba Balázsi

Received: 20 December 2022
Revised: 29 December 2022
Accepted: 5 January 2023
Published: 10 January 2023

1. Introduction

The seismic rehabilitation of existing structures is one of the main topics in the Structural and Seismic Engineering fields concerning many earthquake-prone countries. The requirement of economical and effective retrofit techniques led researchers to develop innovative systems able to limit, or completely avoid, structural damage during seismic events [1,2]. As reported by Soong et al. [3], Passive Energy Dissipation (PED) devices are largely diffuse as retrofit systems and are capable of increasing the energy dissipation in the structural system in which they are installed. The most common principles in which a PED device operates are the yielding of metals, frictional sliding, and deformation of viscoelastic fluid.

Above all the listed systems, the cheapest and simplest PED devices are the ones based on friction and during the last decades, various typologies of Friction Dampers (FDs) have been developed and successfully applied [4–8]. These devices are usually composed of an assembly of several plates coupled with high-strength bolts. The plates that are responsible for the energy dissipation are usually called friction pads and the global FD response is set by varying the bolt torque and, consequently, the nominal load that keeps the friction pads coupled. A FD can be identified as a tribological system thanks to the presence of two contact surfaces (two friction pads in contact) under a constant nominal load (the bolt torque). As a result, the main factors that describe those tribological systems are roughness, hardness, and superficial finishing, especially in the presence of superficial treatments [9,10].

Surface roughness is still one of the most investigated parameters to understand its influence on the wear behavior of different kinds of materials. Liang et al. [11] investigated

the role of initial surface roughness, observing that higher initial roughness parameters Ra, Rq, and Rku lead to a longer initial steady-state transition period and a lower coefficient of friction (COF).

Surface treatment and modification is a quick and effective solution to improve properties such as corrosion resistance, wear behavior, and fatigue life. In this regard, galvanic electrodepositions of Ni and Zn are widely used to protect steel parts against corrosion [12]. Several authors [13–15] investigated Zn coatings in pin-on-flat and Pin-on-Disk (PoD) dry sliding tests, observing that the low hardness of the Zn layer led to the formation of a tribo-layer that lowered the COF also in the case of high loads and contact pressures. In these works, the Ni percentage in the coating was also evaluated, concluding that the presence of Ni improved both corrosion and wear resistance.

Shot peening is also a deeply investigated solution to improve the fatigue life of steel components by inducing residual compressive stresses [16,17]. Due to the automotive and aerospace application of this treatment, it is interesting to investigate the tribological behavior of shot-peened surfaces. Several authors [18,19] investigated the effect of shot peening pressure on the surface roughness and the mechanical properties and their relationship with the wear behavior of steel. It has been observed that an increment of shot pressure results in an increment of both surface hardness and roughness, while an increment of surface roughness results in a COF increment and wear loss decrement.

Several research groups studied the optimization of FD's mating surfaces [20–22]; however, their research focused on scaled prototypes rather than real devices, limiting the number of investigated surfaces. On the contrary, the execution of PoD tests allows the investigation of several couplings focusing on the tribological characterization of the selected surfaces. To correctly characterize an FD's tribological system, and to obtain COF trends and wear rate (WR) reliable results, the PoD testing conditions need to be set to reproduce the actual conditions. Brake systems are a valuable analogy since the behavior of their tribological system is similar to the FDs one. Sinha et al. [23] observed that PoD tests are an economical and efficient system, and the tribometer's setting versatility allows to properly set the involved parameter. More precisely, a pv parameter, obtained by the product between the mean contact pressure p and sliding velocity v, has been reported as a good approximation for the actual condition during the characterization of braking systems [24,25].

In the context of developing an innovative seismic dissipation system, which aims to compromise the steadiness of COF and process costs [26], this work deals with the tribological characterization of a structural steel preliminarily treated by different mechanical and galvanic processes. PoD tests have been performed and set to reproduce the actual condition of the device in development, taking into account the pv parameter and the typical earthquake duration. The study has been addressed to highlight the influence of selected low-cost mechanical and galvanic treatments applied to the structural steel on its tribological behavior, focusing on the steadiness of COF and limited values of the specific wear rate (WR). Section 2 describes the investigated material and treatments, which have been selected considering the lowest cost processes, and the methods adopted to perform the tribological characterization. Section 3 shows the results and comments of the surface characterization and wear tests, while Section 4 collects the final main remarks.

2. Materials and Methods

This study is settled in the context of the development of an innovative FD balancing the steadiness of COF as a function of time/displacement and process costs. The main body of the device in development is made of structural S355JR steel and this material is set as a reference to respect the low-cost requirement. The tribological characterization of the structural steel was carried out by performing tests in a PoD configuration and a reciprocating sliding motion. Specimens consisted of steel S355JR flat-ended cylindrical pins sliding on a rotating disk of the same material. The geometries of both pin and disk are reported in Table 1.

Table 1. Geometric parameters of PoD specimens.

Specimen	Diameter (mm)	Thickness (mm)
Pin	6	32
Disk	165	8

Disks were obtained both by machining and turning, to achieve a nominal roughness Ra of 0.8 µm, and subsequently treated by different low-cost mechanical and galvanic processes. More precisely, electrolytic nickel plating (NI), white electrolytic zinc plating (ZN), and two different shot peening treatments named SP1 and SP2 were considered. The original turned disk (TR) was used as a reference. Figure 1 shows an image of the disks and one of the pins used in the present investigation.

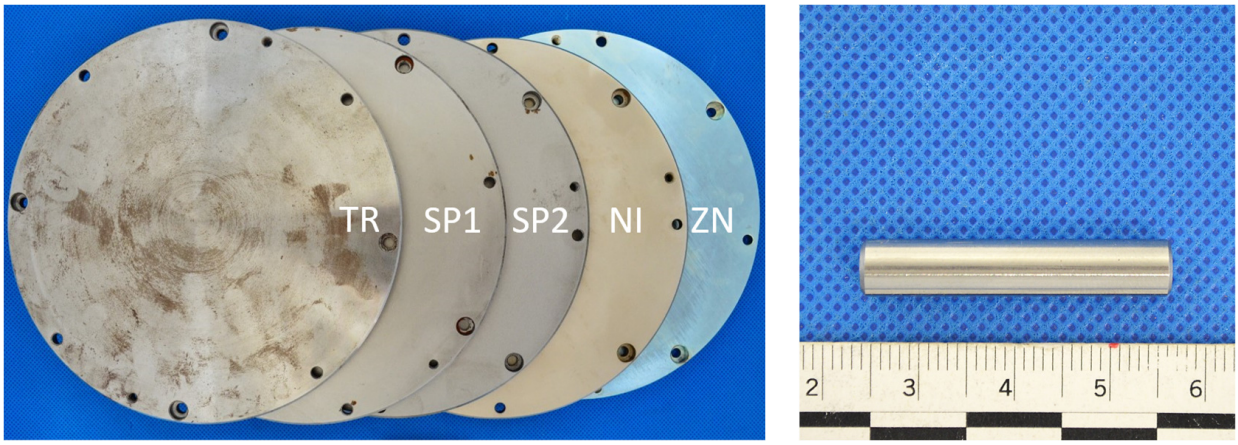

(**a**) (**b**)

Figure 1. Specimens used in the study: (**a**) disks and (**b**) representative pin.

The characterization of the reference material and the additional treatments were performed on a cross-section of the disks to determine the initial roughness and the treatment thickness. A Talysurf CCI-Lite non-contact 3D profilometer (Taylor Hobson, Leicester, UK) was used to evaluate the average roughness of each specimen over three different measurements. In accordance with the literature [11,27], the samples' surface roughness was evaluated by calculating the *Ra* parameter following the UNI EN ISO 25178-2:2022 standard [28], while evaluation length and cut-off following the UNI EN ISO 21920-3:2021 [29]. *Ra* is defined as the mean difference in height from the mean height on the considered profile. An optical microscope Leica dMi8 A (Leica Microsystem, Wetzlar, Germany) with acquisition software LAS v4.13 was used to measure and evaluate the average thickness of each treatment over ten different measurements.

Hardness measurements were carried out by instrumented nanoindentation, using different indenters according to the literature [13,30]. An AntonPaar NHT^2 nanoindenter (Anton Paar GmbH, Graz, Austria) with a Berkovich penetrator was used to determine ZN and NI hardness, with a preset load of 20 mN with a 2 mN/s loading rate, a 5 s holding time, and a final 2 mN/s de-loading rate step. Five indentions were made in each test for statistical analysis and consistency inspection. The hardness and the reduced elastic modulus were calculated by fitting the load-displacement (P–h) curve using the Oliver–Pharr method. A Fischerscope HM2000 (Helmut-Fischer GmbH, Sindelfingen, Germany) with a Vickers indenter was used to determine the hardness along the cross-section of the shot-peened samples SP1 and SP2. A 20 mN load was applied with a 2 mN/s loading rate, maintained for a 5 s holding time and a final 2 mN/s de-loading rate step. To evaluate the hardness as a function of the depth along the cross-section an indentation profile with 30 µm steps was carried out. The hardness was calculated from three measurements in

each position. To compare the hardness values, the resultant Berkovich's hardness values were converted to the Vickers scale according to UNI EN ISO 14577-1:2015 [31].

Wear tests were performed to evaluate COF over time and the WR of disks and pins for each selected coupling. A TR20-LE (Ducom Instruments, Bengaluru, India) tribometer set on pin-on-disk reciprocating configuration and software WinDucom were used to monitor the COF values over time. Tests were performed under dry conditions and at room temperature, in accordance with the ASTM G99-17 standard. During the tests, pins were subjected to a 50 N vertical load while disks were rotating at 1 Hz and 2 Hz oscillatory frequencies. The setting was calibrated to reproduce the actual condition of the FD device and assume disk rotation frequencies typical of the structural system in which a FD is usually installed. In the real use conditions, the typical values of the pv parameter for the FD (pv_{FD}) under development range between 0.10 and 0.20 [26]. Setting a circular arc pin track with an average of 54 mm arc length and considering oscillatory frequencies of 1 Hz and 2 Hz, the associated maximum linear speed equals 0.111 m/s and 0.222 m/s, respectively. Applying a vertical 50 N load, the pv parameter for the PoD test (pv_{PoD}) reaches values similar to the pv_{FD} ones, registering a pv_{PoD}/pv_{FD} ratio close to the unit.

A Talysurf CCI-Lite non-contact 3D profilometer was used to analyze the disk's wear tracks and determine the disk's specific wear rate (WR_d). More precisely, WR_d (expressed in mm^3/Nm) was obtained using Equation (1)

$$WR_d = \frac{\Delta V}{S_{tot}F} = \frac{AS}{S_{tot}F} \quad (1)$$

where:

- ΔV is the disk's volume loss expressed in mm^3;
- A is the wear track's area expressed in mm^2;
- S is the wear track's length expressed in mm;
- S_{tot} is the total sliding length expressed in m;
- F is the applied load expressed in N.

A Kern ABT 100-5NM (Kern, Balingen, Germany) analytical balance, with an accuracy resolution of 0.01 mg, was used to measure the pin's mass loss and to determine the pin's specific wear rate (WR_p). Pins were weighed before and after each PoD test, evaluating the average pin's mass loss over three different measurements. More precisely, WR_p (expressed in mm^3/Nm) was obtained using Equation (2)

$$WR_p = \frac{\Delta g}{\rho S_{tot}F} \quad (2)$$

where:

- Δg is the pin's mass loss expressed in g;
- ρ is the pin's mass density expressed in g/mm^3 (in the case of S355JR steel it can be assumed as 7870 kg/m^3);
- S_{tot} is the total sliding length expressed in m;
- F is the applied load expressed in N.

The wear testing procedure has been set by taking into account the typical break-in curve shape of treated surfaces in Figure 2. Blau [32] reported that, commonly, treated surfaces are characterized by two steady-state stages with associated transition times (t_{tr}), defined as the time needed to reach a steady-state stage, and the mean steady-state COF values (COF_{st}) registered during the steady-state stage. The first steady-state stage is originated from the treated surface (a harder layer, a coating layer, or trapped coating wear debris) and coincides with the surface treatment useful life [33], lasting until the treated layer is completely removed. The surface treatment useful life ends as the friction coefficient unstably increases after the steady-state stage. Once the substrate is exposed to wear, the second steady-state stage is reached and lasts until the end of the test.

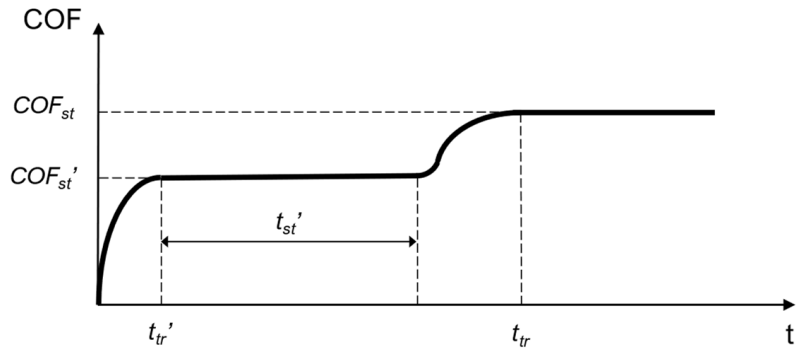

Figure 2. Curve shape of the most common break-in of treated surfaces.

To evaluate the consistency of COF, the mean steady-state COF value is associated with a coefficient of variation defined as the ratio between the mean standard deviation and mean COF value in the steady-state stage.

The wear testing procedure consisted of two different phases with different duration and purposes. In the first phase (P1), 900 s duration long tests (LT) were performed to investigate the overall COF behavior with time and to evaluate an adequate run-in period to reach COF_{st} values. To use a constant methodology, the run-in period was chosen as the biggest t_{tr} from all the investigated couplings, increased by 50% to take account of the variability of the results. In the second phase (P2), interrupted tests (IT) were performed to evaluate the consistency of COF. Each interrupted test had a run-in (IT-RI) stage of 300 s duration and a group of five subsequent shorter stages (IT-S), whose duration was selected considering typical earthquake duration, to detect an eventual degradation of COF due to subsequent sliding events. A total of four duration groups were selected (30 s, 60 s, 90 s, and 120 s) for a total of four different interrupted tests. Wear test duration is summarized in Table 2.

Table 2. Wear test duration summary.

Phase	Test	Total Sliding (s)	Run-In Stage (s)	Short Stage (s)
P1	LT	900	-	-
P2	IT30	450	300	30
	IT60	600	300	60
	IT90	750	300	90
	IT120	900	300	120

3. Results and Discussion

3.1. Characterization of the Surface Roughness of the Processes

Figure 3 shows the tridimensional topography reconstruction of the investigated disks used to evaluate their initial roughness (*Ra*), listed in Table 3. TR condition shows a segmented texture (see Figure 3a), with an average *Ra* value of 0.73 µm, which is close to the nominal roughness. NI, SP1, and SP2 conditions show a non-periodical texture (see Figure 3b, Figure 3d, and Figure 3e, respectively), with *Ra* values that range between 0.97 and 2.20 µm. ZN condition (see Figure 3c) shows a topography comparable with the reference TR, with an average *Ra* value of 0.53 µm. NI, SP1, and SP2 exhibit the highest deviation from the reference TR topography, with a significant change in both texture morphology and roughness. On the contrary, ZN exhibits only a decrement compared to the TR initial roughness.

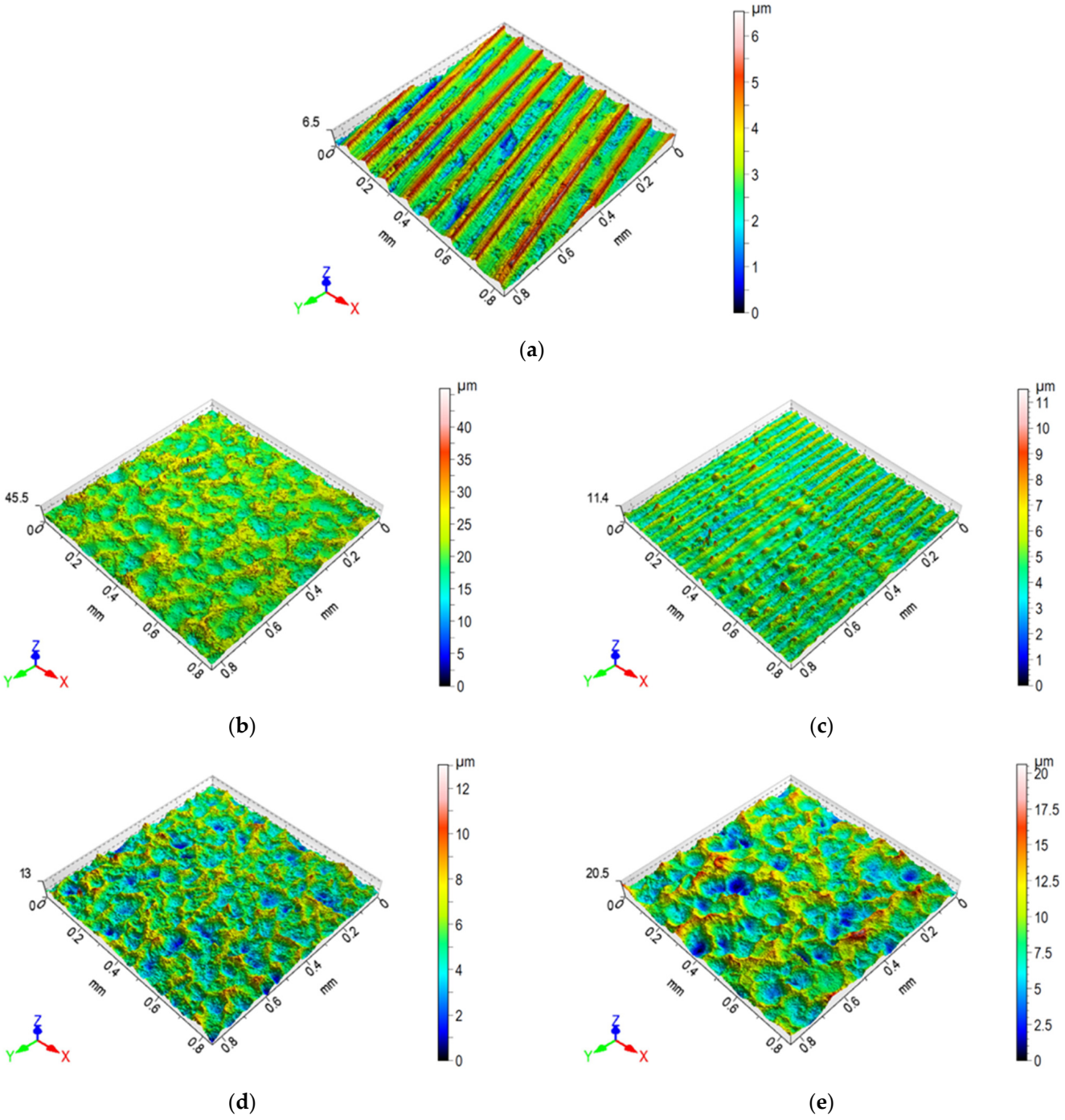

Figure 3. Tridimensional topography reconstruction of the investigated disks: (**a**) TR, (**b**) NI, (**c**) ZN, (**d**) SP1, and (**e**) SP2.

Table 3. Roughness values (*Ra*) of the disks and thickness values (*t*) of the galvanizing treatments.

Conditions	*Ra* (µm)	*t* (µm)
TR	0.73 ± 0.01	-
NI	2.20 ± 0.10	9.1 ± 0.9
ZN	0.52 ± 0.07	Max: 8.2 ± 0.9 Min: 4.8 ± 1.3
SP1	0.97 ± 0.03	-
SP2	1.77 ± 0.12	-

Figure 4a,b shows the optical micrographs of the cross-sections for NI and ZN disks, respectively, used to evaluate the thickness of the coatings (t), listed in Table 3. Despite the irregular superficial texture, NI displays an almost constant thickness that is 9.1 µm on average. On the contrary, the thickness of ZN varies with values ranging between 4.8 and 8.2 µm in correspondence to the valleys and picks, respectively, resulting from the turning. This is responsible for the lower roughness of the ZN specimen compared to the reference TR, as previously described during the tridimensional topography analysis.

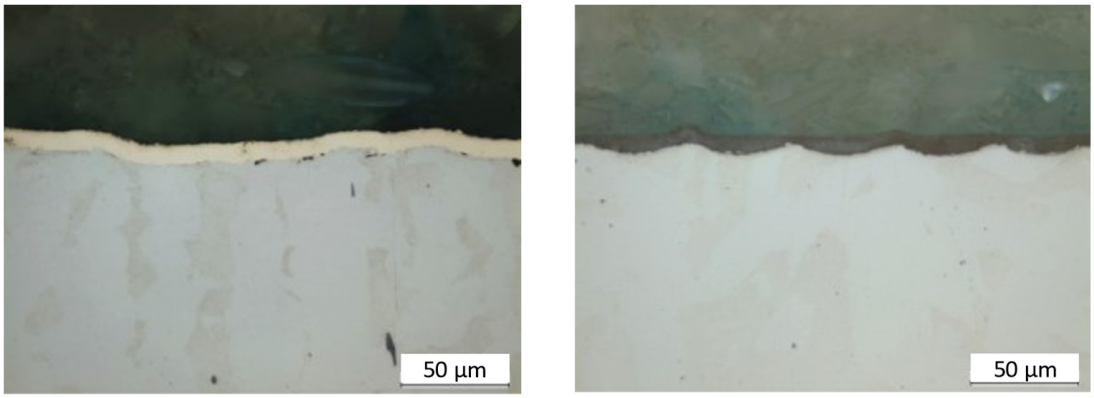

Figure 4. Optical micrographs for thickness measurements of (**a**) NI and (**b**) ZN conditions.

Figure 5 shows the Vickers hardness values through the cross-section of SP1 and SP2 disks, over three different replicas. As the impact of the shots with the specimen's surface causes plastic deformation, the hardness reaches its largest values in the sub-superficial zone of the sample and gradually reduces with depth [18]. SP2 showed a sub-superficial hardness (452 ± 31 HV) higher than SP1 (320 ± 17 HV), but in both cases that increment faded between 75 and 100 µm of depth. It is worth noting that, a large variation of the results is shown; however, this variation is compatible with the ones registered by Trung et al. [18]. The presence of the different microstructural constituents along the cross-section is easily detectable when a 20 mN load is used, resulting in a higher variation of the registered data.

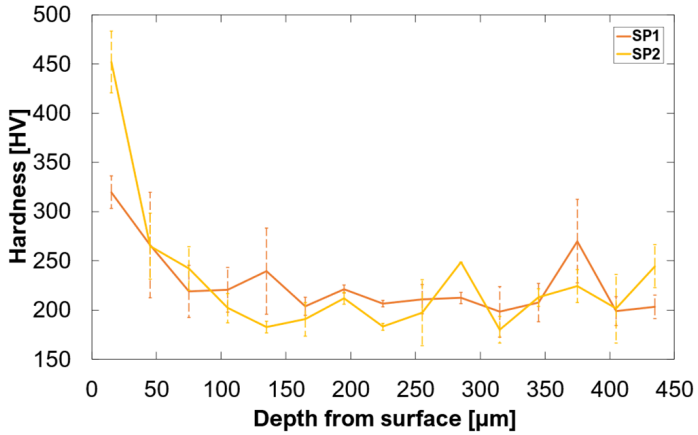

Figure 5. Cross-section hardness variation as a function of depth of SP1 and SP2 conditions.

Vickers hardness values for each considered treated surface are listed in Table 4. According to UNI ISO 14577-1 [31], H_{IT} values for NI and ZN were converted in HV to allow the comparison between the sub-superficial properties of all the surfaces. Based on the experimental data, NI showed the highest hardness and, on the contrary, ZN the lowest one confirming literature data [13,14,30].

Table 4. Values of sub-superficial Vickers hardness of the studied surfaces (HV).

Sample	TR	NI	ZN	SP1	SP2
Hardness (HV)	228 ± 45	607 ± 59	60 ± 8	452 ± 31	320 ± 17

3.2. Wear Tests

P1 LT tests were performed to evaluate an adequate running-in period for the following P2 tests. Figure 6a,b shows the average evolution of COF for the tests performed at 1 Hz and 2 Hz, respectively, over five different replicas. Table 5 lists the transition times t_{tr}' and t_{tr}, the first steady-state duration t_{st}', the mean steady-state COF values COF_{st}' and COF_{st} and their coefficients of variation cv_{COF}' and cv_{COF}.

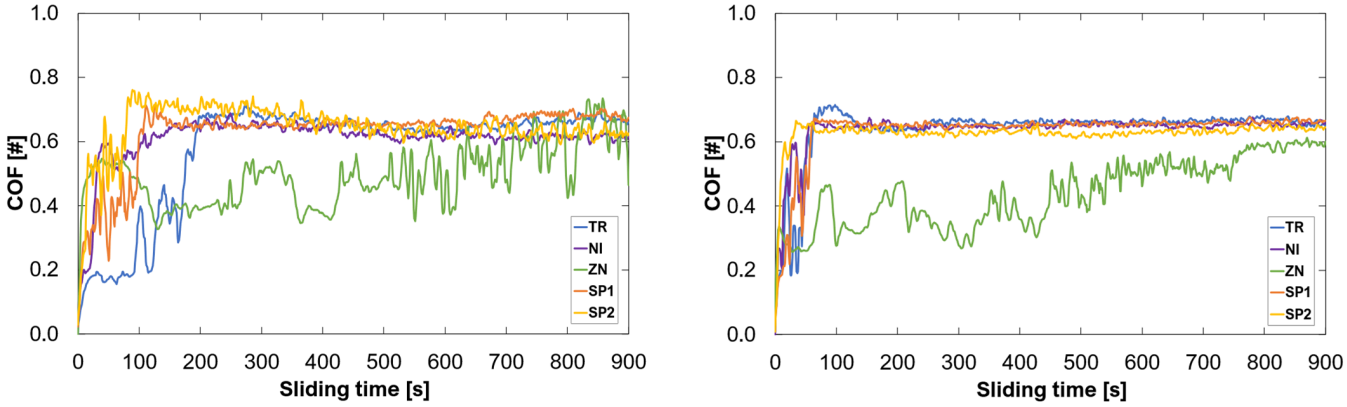

Figure 6. COF evolution during LT tests: (**a**) 1 Hz sliding frequency and (**b**) 2 Hz sliding frequency.

Table 5. LT tests summary: frequency (f), transition time (t_{tr}), steady COF (COF_{st}), and COF's coefficient of variation (cv_{COF}) values.

Condition	f (Hz)	t_{tr}' (s)	t_{st}' (s)	COF_{st}' (#)	$cv_{COF,st}'$	t_{tr} (s)	COF_{st} (#)	$cv_{COF,st}$
TR	1	-	-	-	-	195	0.66	2.7%
	2	-	-	-	-	65	0.66	2.1%
NI	1	30	70	0.56	4.2%	100	0.63	3.0%
	2	15	35	0.50	13.5%	195	0.65	1.1%
ZN	1	10	615	0.45	14.0%	>900	-	-
	2	5	510	0.37	17.3%	750	0.59	2.4%
SP1	1	30	65	0.40	6.8%	110	0.66	2.4%
	2	25	20	0.43	14.5%	60	0.66	1.0%
SP2	1	15	55	0.53	11.6%	80	0.66	5.8%
	2	10	15	0.55	6.6%	30	0.63	1.6%

TR condition reaches only one steady-state stage at both sliding frequencies, with COF_{st} values around 0.66 both at 1 Hz and 2 Hz. This behavior is typical of steel-steel couplings in dry sliding conditions [32].

NI, SP1, and SP2 conditions display similar overall behavior, registering two similar steady-state stages. The first steady-state registers t_{st}' values around 63 s and 23 s at 1 Hz and 2 Hz, respectively, with COF_{st}' values around 0.49 both at 1 Hz and 2 Hz. The second steady-state registers COF_{st} values around 0.65 both at 1 Hz and 2 Hz. It is worth noting that the first steady-state stages exhibit higher values of coefficient of variation ($cv_{COF,st}'$) with respect to the second steady-state ones ($cv_{COF,st}$). The presence of the treatment's surfaces produces a higher COF variation during the sliding, with a consequent less stable

response, while after the treatment's surfaces removal, NI, SP1, and SP2 conditions behave more steadily and similarly to the TR condition. Moreover, during the first steady-state stage, the SP2 condition exhibits a higher $COF_{st}{}'$ value with respect to SP1 condition, as well as with lower $t_{tr}{}'$ and $t_{st}{}'$ values. This different behavior during the first steady-state stage is caused by higher SP2 superficial hardness with respect to SP1 (see Figure 5), as already registered by several studies on shot peening [18,19]. After the harder cross-section portion removal, during the second steady-state stage, SP1 and SP2 behave more similarly.

ZN condition reaches one steady-state stage at 1 Hz and two steady-state stages at 2 Hz. The first steady-state reached both sliding frequencies and registered $t_{st}{}'$ values around 615 s and 510 s at 1 Hz and 2 Hz, respectively, with $COF_{st}{}'$ values around 0.45 and 0.37 at 1 Hz and 2 Hz, respectively. The second steady-state, reached only at 2 Hz, registers COF_{st} values around 0.59. As previously observed for NI, SP1, and SP2, the first steady-state stages exhibit higher values of coefficient of variation ($cv_{COF,st}{}'$) with respect to the second steady-state ones ($cv_{COF,st}$). The presence of the zinc wear particles trapped between the disk and the pins produces a higher COF variation during the sliding, with a consequent less stable response. After the removal of both surface treatments, the ZN condition behaves more steadily than NI and similarly to the TR condition. It is worth noting that ZN registers the longer first steady-state stage above all investigated conditions, indicating that zinc wear particles remain trapped between the disk and the pins longer with respect to the other treatments.

In summary, during LT tests the conditions NI, SP1, and SP2 exhibit lower t_{tr} values with respect to the reference TR ones, especially during 1 Hz sliding tests while during 2 Hz sliding tests, due to the sliding velocity increment, this difference is insignificant. Consequently, NI, SP1, and SP2 conditions only affect t_{tr}, while the average COF_{st} values remain unchanged and $cv_{COF,st}$ are slightly reduced. Concerning the shot peened specimens, SP2 registered a slight increment of COF_{st} and decrement of t_{tr} with respect to SP1; a similar behavior was registered in the work of Khun et al. [19], observing that a roughness increment by shoot peening is associated with an increment of COF values. The condition ZN exhibits a higher t_{tr} and lower COF_{st} values with respect to the reference TR ones, both at 1 Hz and 2 Hz. Consequently, ZN affects both t_{tr} and COF_{st} values resulting in more effectiveness with respect to the other investigated treatments, however, $cv_{COF,st}$ registers a significant increment, especially at a 1 Hz sliding frequency, resulting in less stability with respect to the other investigated treatments. ZN behavior is caused by the formation of a transfer film in which the wear zinc debris are trapped between the pin and the disk acting as a lubricant, as already registered by Sriraman et al. [14], until the complete failure of the coating.

Considering the results of the P1 phase and to ensure the achievement of the COF's steady stages, the P2 IT-RI test duration was set at 300 s. It is worth noting that the transition time of ZN is much longer than 300 s, consequently during the P2 tests, ZN evaluation is focused on the stability of its first steady-stage state, in which the effects of the treatment are more significant.

Figure 7a,b shows the average COF evolution during the IT-RI stages, performed at 1 Hz and 2 Hz, respectively, over five replicas, while Table 6 lists the transition times $t_{tr}{}'$ and t_{tr}, the first steady-state duration $t_{st}{}'$, the mean steady-state COF values $COF_{st}{}'$ and COF_{st}, and their coefficients of variation $cv_{COF}{}'$ and cv_{COF}.

TR condition reaches only one steady-state stage at both sliding frequencies COF_{st} values around 0.71 and 0.67 at 1 Hz and 2 Hz, respectively. TR behavior, as well as the COF_{st} values are close to P1 results, and consequently, the same observation remains valid.

NI, SP1, and SP2 conditions display similar overall behavior, registering two similar steady-state stages. The first steady-state registers $t_{st}{}'$ values around 58 s and 22 s at 1 Hz and 2 Hz, respectively, with $COF_{st}{}'$ values around 0.51 and 0.52 at 1 Hz and 2 Hz, respectively. The second steady-state registers COF_{st} values around 0.67 and 0.66 at 1 Hz and 2 Hz, respectively. NI, SP1, and SP2 behavior, as well as the COF_{st} values are close to P1 results, and consequently, the same observation remains valid. However, it is worth

noting that, at the end of the IT-RI stage, NI, SP1, and SP2 reach the second steady-state; as a result, in the following tests, their behavior is expected to be close to the TR condition. Moreover, NI conditions exhibit lower $cv_{COF,st}$ values with respect to the other investigated treatments, resulting in more stability during IT-RI tests.

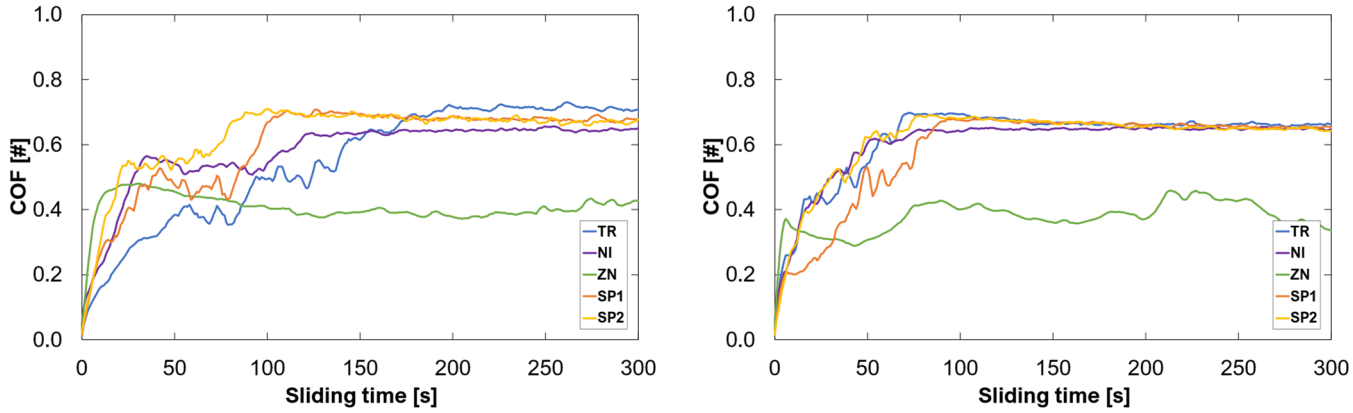

Figure 7. Evolution of COF during IT-IR tests, run-in stage: (**a**) 1 Hz and (**b**) 2 Hz sliding frequency.

Table 6. IT-RI stage tests transition time, steady COF values, and COF's coefficient of variation.

Condition	f (Hz)	t_{tr}' (s)	t_{st}' (s)	COF_{st}' (#)	$cv_{COF,st}'$	t_{tr} (s)	COF_{st} (#)	$cv_{COF,st}$
TR	1	-	-	-	-	175	0.71	1.4%
	2	-	-	-	-	70	0.67	1.9%
NI	1	25	75	0.53	3.0%	120	0.64	1.0%
	2	25	15	0.51	4.0%	70	0.65	0.7%
ZN	1	5	295	0.41	7.1%	>300	-	-
	2	5	295	0.38	11.2%	>300	-	-
SP1	1	30	60	0.48	5.6%	100	0.68	1.3%
	2	45	30	0.51	5.8%	85	0.66	1.2%
SP2	1	20	40	0.54	2.6%	85	0.68	1.7%
	2	25	20	0.50	5.4%	75	0.66	2.0%

The ZN condition reaches only the first steady-state stage at both sliding frequencies, with t_{st}' values around 295 s both at 1 Hz and 2 Hz, and COF_{st}' values around 0.48 and 0.38 at 1 Hz and 2 Hz, respectively. ZN behavior, as well as the COF_{st} values are close to P1 results, and consequently, the same observation remains valid. However, it is worth noting that ZN reaches a higher $cv_{COF,st}'$ with respect to the other investigated treatment, resulting in less stability during IT-RI tests.

In summary, during IT-RI tests, the conditions NI, SP1, and SP2 only affect t_{tr}, while the average COF_{st} values remain unchanged and $cv_{COF,st}$ are slightly reduced, especially for NI. On the contrary, ZN affects both t_{tr} and COF_{st} values resulting in more effectiveness with respect to the other investigated treatments, however cv_{COF} registers a significant increment at both selected sliding frequencies, resulting in less stability with respect to the other investigated treatments.

Figure 8a–d shows the average COF variation during the IT-S stages, of 30 s, 60 s, 90 s, and 120 s duration, respectively, over five subsequent repetitions performed at 1 Hz sliding frequency. Table 7 lists the transition time (t_{tr}), the average steady COF values (COF_{st}), and its coefficient of variation (cv_{COF}) for the IT-S tests performed at a 1 Hz sliding frequency.

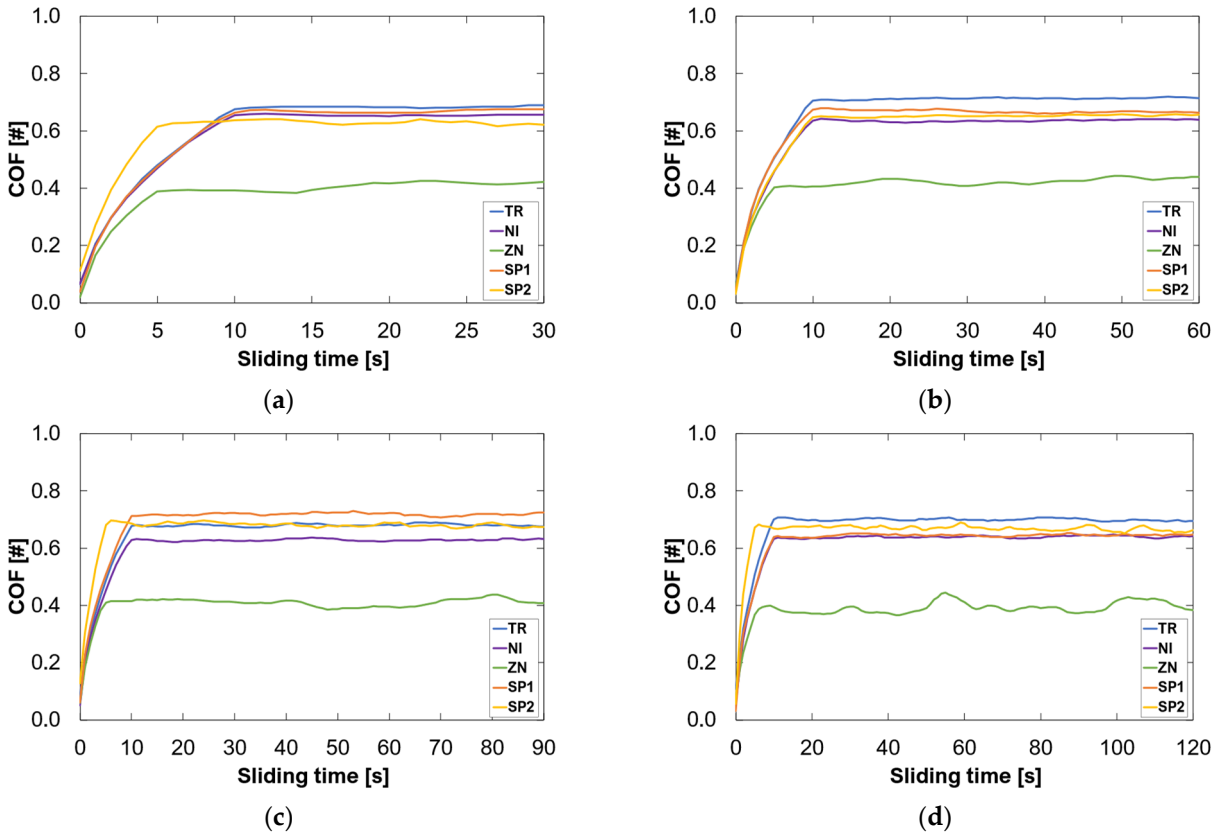

Figure 8. Evolution of COF during IT-S tests at a 1 Hz sliding frequency: (**a**) 30 s (IT30), (**b**) 60 s (IT60), (**c**) 90 s (IT90), and (**d**) 120 s (IT120).

Table 7. Variation of t_{tr}, COF_{st}, and of cv_{COF} at 1 Hz sliding frequency.

Condition	Test	t_{tr} (s)	COF_{st} (#)	$cv_{COF,st}$
TR	IT30	10	0.68	1.1%
	IT60	10	0.71	1.1%
	IT90	10	0.68	2.1%
	IT120	10	0.70	2.8%
NI	IT30	10	0.65	2.1%
	IT60	10	0.64	1.1%
	IT90	10	0.63	1.3%
	IT120	10	0.64	1.2%
ZN	IT30	5	0.41	13.2%
	IT60	5	0.42	6.4%
	IT90	5	0.41	9.3%
	IT120	5	0.39	12.5%
SP1	IT30	10	0.67	1.6%
	IT60	10	0.67	3.1%
	IT90	10	0.72	1.9%
	IT120	10	0.64	1.4%
SP2	IT30	5	0.63	1.8%
	IT60	10	0.65	1.3%
	IT90	5	0.68	3.5%
	IT120	5	0.67	4.0%

TR, NI, SP1, and SP2 displayed similar overall behavior, immediately reaching the final steady-stage state with t_{tr} values ranging between 5 and 10 s, COF_{st} values ranging between 0.63 and 0.71, and $cv_{COF,st}$ ranging between 1.1% and 4.0%. As previously underlined, at the end of the IT-RI stage the conditions NI, SP1, and SP2 reached the second and final

steady-state stage, resulting in the complete removal of the surface treatment and exhibiting a behavior close to the TR condition during IT-S tests. However, it is worth noting that NI conditions exhibit lower $cv_{COF,st}$ values with respect to the other investigated treatments, resulting in more stability during IT-S tests.

ZN reaches only the first steady-state stage state with t_{tr} values around 5 s, COF_{st} values ranging between 0.39 and 0.42 and $cv_{COF,st}$ ranging between 6.4% and 13.2%. As previously underlined, at the end of the IT-RI stage the condition ZN reached the first steady-state stage, resulting in incomplete removal of the surface treatment. Therefore, ZN reaches a higher $cv_{COF,st}$ with respect to the other investigated treatment, resulting in less stability during IT-S tests.

Figure 9a–d shows the average COF variation during the IT-S stages, of 30 s, 60 s, 90 s, and 120 s duration, respectively, over five subsequent repetitions performed at a 2 Hz sliding frequency. Table 8 lists the transition time (t_{tr}), the average steady COF values (COF_{st}), and its coefficient of variation (cv_{COF}) for the IT-S tests performed at a 2 Hz sliding frequency.

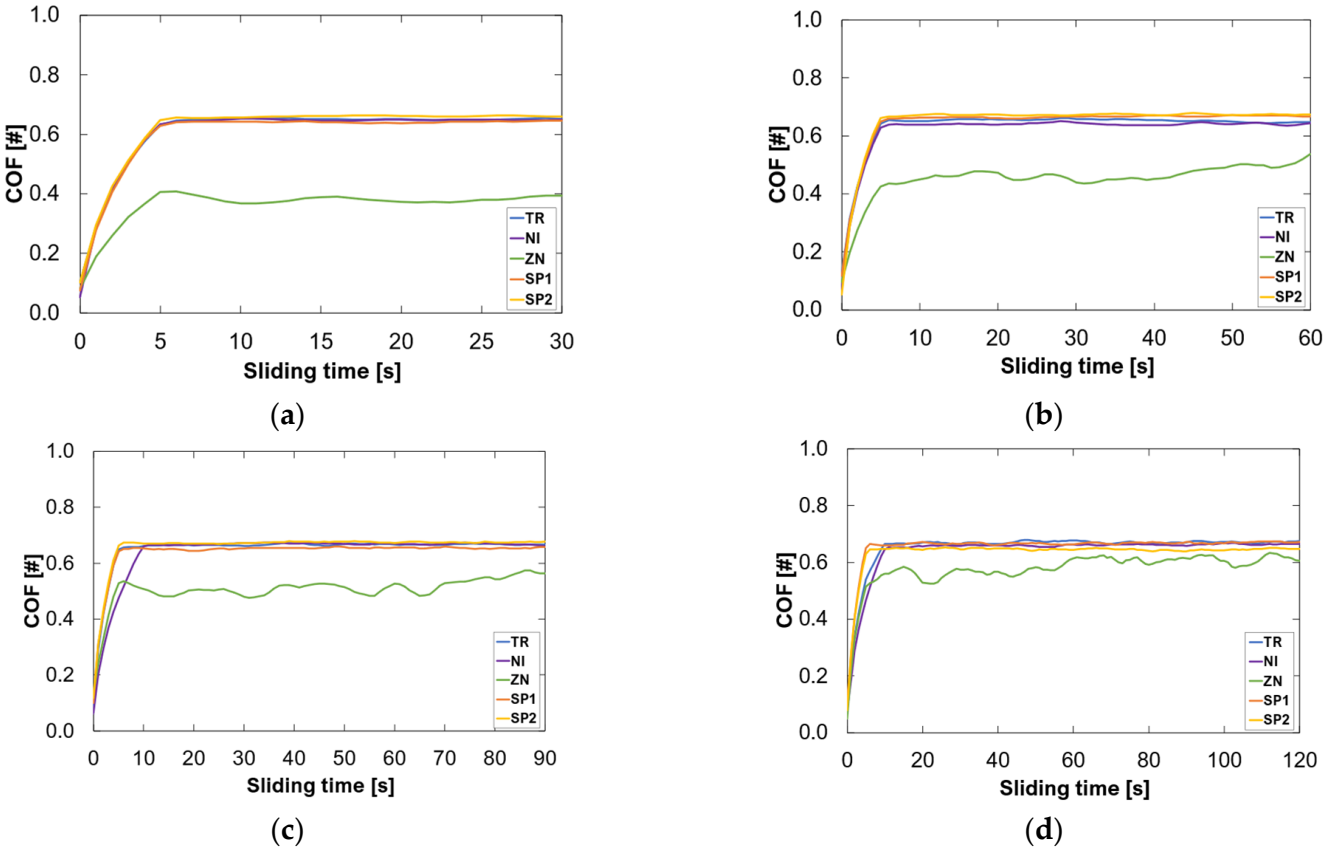

Figure 9. COF vs time curves in tribological IT tests for 2 Hz: (**a**) 30 s (IT30), (**b**) 60 s (IT60), (**c**) 90 s (IT90), and (**d**) 120 s (IT120).

TR, NI, SP1, and SP2 displayed similar overall behavior, immediately reaching the final steady-stage state with t_{tr} values ranging between 5 and 10 s, COF_{st} values ranging between 0.64 and 0.67, and $cv_{COF,st}$ ranging between 0.7% and 1.6%. As previously underlined, at the end of the IT-RI stage the conditions NI, SP1, and SP2 reached the second and final steady-state stage, resulting in the complete removal of the surface treatment and exhibiting a behavior close to the TR condition during IT-S tests. However, it is worth noting that NI conditions exhibit lower $cv_{COF,st}$ values with respect to the other investigated treatments, resulting in more stability during IT-S tests.

Table 8. Variation of t_{tr}, COF_{st}, and of cv_{COF} at 2 Hz sliding frequency.

Condition	Test	t_{tr} (s)	COF_{st} (#)	$cv_{COF,st}$
TR	IT30	5	0.65	1.3%
	IT60	5	0.65	1.2%
	IT90	5	0.67	1.3%
	IT120	10	0.67	1.6%
NI	IT30	5	0.65	0.7%
	IT60	5	0.64	1.2%
	IT90	10	0.67	0.9%
	IT120	10	0.66	1.2%
ZN	IT30	5	0.38	24.1%
	IT60	5	0.47	23.9%
	IT90	5	0.52	15.5%
	IT120	5	0.59	12.8%
SP1	IT30	5	0.64	1.4%
	IT60	5	0.67	0.9%
	IT90	5	0.65	1.2%
	IT120	5	0.67	1.3%
SP2	IT30	5	0.64	1.4%
	IT60	5	0.67	0.9%
	IT90	5	0.67	1.0%
	IT120	5	0.65	1.2%

ZN reaches only the first steady-state stage state with t_{tr} values around 5 s, COF_{st} values ranging between 0.38 and 0.59, and $cv_{COF,st}$ ranging between 15.5% and 24.1%. As previously underlined, at the end of the IT-RI stage the condition ZN reached the first steady-state stage, resulting in the incomplete removal of the surface treatment. Therefore, ZN reaches a higher $cv_{COF,st}$ with respect to the other investigated treatments, resulting in less stability during IT-S tests. Moreover, it is worth noting that an increment in IT-S test duration is associated with an increment of COF_{st} values, meaning that at the end of the longer tests the zinc layer is almost completely removed, reaching the proximity of the second steady-state stage.

In summary, during IT-S stages, NI, SP1, and SP2 exhibit similar t_{tr} and COF_{st} values as the reference TR ones, with COF_{st} values remaining almost constant with the subsequent repetitions and sliding time increments. Consequently, once the second steady-state stage is reached, NI, SP1, and SP2 insignificantly affect the reference TR behavior, registering only a slight $cv_{COF,st}$ value decrement, especially for NI. On the contrary, ZN exhibits similar t_{tr} and lower COF_{st} values as the reference TR ones, with COF_{st} values incrementing with the subsequent repetitions and sliding time increment, especially for 2 Hz sliding frequency tests. Consequently, ZN affects only COF_{st} values resulting in more effectiveness with respect to the other investigated treatments, however, the steadiness with the repetition and sliding time increment significantly decreases.

The results of the specimens' wear tracks evaluation and specific wear rate are listed in Tables 9 and 10 for P2-IT tests performed at 1 Hz and 2 Hz, respectively, in terms of wear tracks width (w), wear tracks depth (d), and specific wear rate on the disks (WR_d) and on the pins (WR_p).

Table 9. Variation of w, d, WR_d, and on the pins WR_p at 1 Hz sliding frequency.

Condition	Test	w (mm)	d (μm)	WR_d (mm^3/Nm)	WR_p (mm^3/Nm)
TR	IT30	6.04	87.50	6.13×10^{-3}	6.43×10^{-3}
	IT60	6.03	100.80	5.56×10^{-3}	5.87×10^{-3}
	IT90	6.00	153.80	7.28×10^{-3}	6.16×10^{-3}
	IT120	6.05	159.60	7.12×10^{-3}	6.39×10^{-3}
NI	IT30	6.00	105.88	7.78×10^{-3}	4.08×10^{-3}
	IT60	6.11	111.97	6.72×10^{-3}	3.76×10^{-3}
	IT90	6.09	135.07	6.11×10^{-3}	3.34×10^{-3}
	IT120	6.21	124.60	5.20×10^{-3}	3.54×10^{-3}
ZN	IT30	4.63	30.10	9.20×10^{-4}	3.52×10^{-5}
	IT60	5.27	36.70	1.11×10^{-3}	5.88×10^{-5}
	IT90	5.14	25.80	5.00×10^{-4}	3.89×10^{-5}
	IT120	3.76	38.30	5.00×10^{-4}	8.05×10^{-5}
SP1	IT30	5.99	111.50	8.26×10^{-3}	3.18×10^{-3}
	IT60	5.96	132.80	7.81×10^{-3}	3.42×10^{-3}
	IT90	6.05	152.17	6.81×10^{-3}	3.18×10^{-3}
	IT120	6.18	161.33	6.66×10^{-3}	2.99×10^{-3}
SP2	IT30	5.94	106.50	8.02×10^{-3}	3.17×10^{-3}
	IT60	5.95	132.63	7.86×10^{-3}	3.23×10^{-3}
	IT90	6.00	121.20	5.79×10^{-3}	2.87×10^{-3}
	IT120	6.09	139.17	5.98×10^{-3}	2.49×10^{-3}

Table 10. Variation of w, d, WR_d, and on the pins WR_p at 2 Hz sliding frequency.

Condition	Test	w (mm)	d (μm)	WR_d (mm^3/Nm)	WR_p (mm^3/Nm)
TR	IT30	6.09	156.10	6.82×10^{-3}	5.44×10^{-3}
	IT60	6.06	182.30	5.91×10^{-3}	5.48×10^{-3}
	IT90	6.13	197.60	5.38×10^{-3}	4.83×10^{-3}
	IT120	6.12	227.20	5.33×10^{-3}	4.85×10^{-3}
NI	IT30	5.97	146.27	5.46×10^{-3}	5.74×10^{-3}
	IT60	6.08	174.07	5.26×10^{-3}	5.25×10^{-3}
	IT90	6.11	204.50	5.08×10^{-3}	5.63×10^{-3}
	IT120	6.14	203.83	4.47×10^{-3}	4.12×10^{-3}
ZN	IT30	5.72	50.30	1.19×10^{-3}	5.44×10^{-5}
	IT60	5.69	58.40	1.18×10^{-3}	5.73×10^{-4}
	IT90	6.11	95.10	1.82×10^{-3}	1.33×10^{-3}
	IT120	6.06	117.50	2.06×10^{-3}	1.36×10^{-3}
SP1	IT30	6.06	136.57	5.71×10^{-3}	4.47×10^{-3}
	IT60	6.09	173.83	5.59×10^{-3}	4.77×10^{-3}
	IT90	6.04	236.57	6.05×10^{-3}	4.10×10^{-3}
	IT120	5.71	205.30	4.35×10^{-3}	3.54×10^{-3}
SP2	IT30	5.97	130.87	4.50×10^{-3}	3.97×10^{-3}
	IT60	6.06	187.30	5.58×10^{-3}	4.04×10^{-3}
	IT90	6.05	189.20	4.81×10^{-3}	3.95×10^{-3}
	IT120	6.01	179.60	3.72×10^{-3}	3.41×10^{-3}

All the conditions show similar values of w ranging around 6 mm, which match with the pins' diameter, except ZN, which registered lower w values at 1 Hz, ranging between 3.76 and 5.27. The specimens show similar behavior in terms of d increment with the sliding time (see Figure 10), with lower values for IT30 tests and higher values for IT120 tests. The conditions TR, NI, SP1, and SP2 incremented with similar values, ranging from 100 µm and 150 µm for IT30 and IT120, respectively at 1 Hz and from 140 µm and 200 µm for IT30 and IT120, respectively at 2 Hz. It is worth noting that d values of NI, SP1, and SP2 are higher than the respective treatment's layer, confirming the complete removal of the surface treatment and associated final COF values close to the TR condition ones. The ZN condition registers significantly lower values than TR, ranging from 25 µm and 40 µm for IT30 and IT120, respectively, at 1 Hz and from 50 µm and 120 µm for IT30 and IT120, respectively, at 2 Hz. It is worth noting that, while at 1 Hz sliding frequency d are almost constant with the increment of tests duration, at 2 Hz sliding frequency d register an increment with the increment of tests duration. Moreover, despite d values being higher than the treatment layer suggesting the complete removal of the treatment surface, during the IT tests the final COF values are significantly lower than the TR ones. Therefore, zinc wear debris is trapped between the pin and the disk for the test duration due to the lower superficial hardness of ZN (see Table 4).

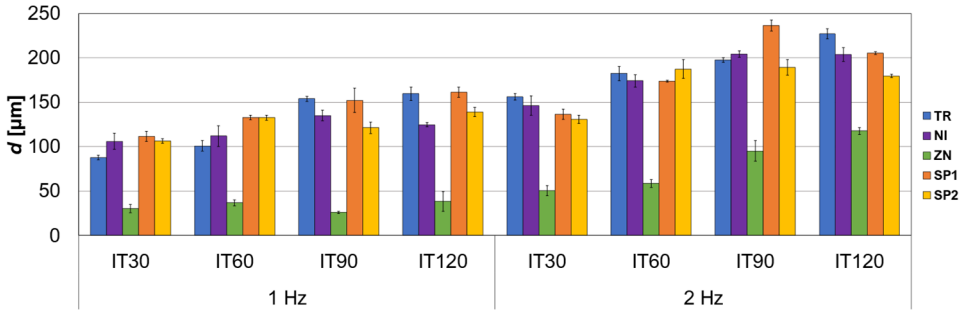

Figure 10. Influence of the duration of the tribological test on wear tracks depth. Error bars indicate the uncertainty of the measurements as standard deviation.

In summary, the wear track dimensions are significantly influenced by the test duration and sliding frequency, especially in terms of track depth, with ZN showing lower values and resulting in less degrading for the disk. However, while TR, NI, SP1, and SP2 show an increment from IT30 to IT120 of 50% both at 1 Hz and 2 Hz sliding frequency, NI shows an increment from IT30 to IT120 of 50% at 1 Hz and of 130% at 2 Hz sliding frequency.

The specific wear rate of the specimens is analyzed both for disks (WR_d) and pins (WR_p). Similar behavior in terms of WR_d decrement with the sliding time (see Figure 11a) was found, with the highest values for IT30 tests and lowest values for IT120 tests, except ZN at 2 Hz behaves the opposite. TR displays the overall highest WR_d values, ranging from 5.33×10^{-3} mm^3/Nm and 7.28×10^{-3} mm^3/Nm, while ZN displays the overall lower WR_d values, ranging from 5.00×10^{-4} mm^3/Nm and 2.06×10^{-3} mm^3/Nm. The conditions show similar behavior in terms of WR_p decrement with the sliding time (see Figure 11b), with the highest values for IT30 tests and lowest values for IT120 tests, except ZN at 2 Hz behaves the opposite. TR shows the overall higher WR_p values, ranging from 4.83×10^{-3} mm^3/Nm and 6.47×10^{-3} mm^3/Nm, while ZN shows the overall lower WR_p values, ranging from 3.52×10^{-5} mm^3/Nm and 1.36×10^{-3} mm^3/Nm.

Hence, the specific wear rate of both disks and pins is significantly influenced by the test duration and sliding frequency, with ZN showing lower values and resulting in less degrading for the disks and the pins. Moreover, while TR shows WR_d values with more resemblance to the NI, SP1, and SP2 ones, TR WR_p values are significantly higher than the NI, SP1, and SP2 ones, especially during the tests performed at a 1 Hz sliding frequency.

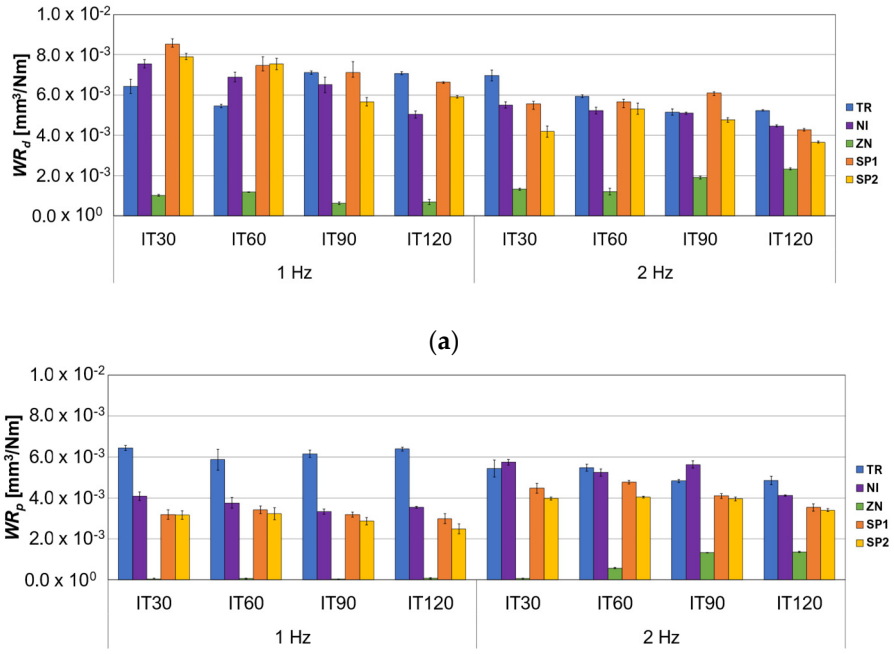

Figure 11. Influence of the duration of the tribological test on the specific wear rate for (**a**) disks and (**b**) pins. Error bars indicate the uncertainty of the measurements as standard deviation.

4. Concluding Remarks

The present work focuses on the tribological characterization of an S355JR structural steel, treated by different mechanical and galvanic processes, analyzed during the development of an innovative FD for seismic protection. The main results in terms of the working window and COF's steadiness with repetitions are summarized as follows:

- NI, SP1, and SP2 conditions show a limited working window in terms of the first steady-state stage, reaching COF_{st} values similar to that of the TR reference condition in less than two minutes.
- ZN condition shows a significant working window in terms of the first steady-state stage, reaching COF_{st} values similar to that of the TR reference condition after more than ten minutes.
- At the studied conditions, NI, SP1, and SP2 treatments show no effective improvement with respect to the TR tribological behavior, despite the increment of overall COF's steadiness with the repetition and sliding time increment.
- At the studied conditions, ZN treatment shows a significative improvement with respect to the TR tribological behavior, despite the decrement in overall COF's steadiness with the repetition and sliding time increment.

The results of this tribological investigation allow the selection of a proper tribological coupling for the innovative FD in development, which is the main goal of the research program. However, scaled PoD tests might not correctly reproduce the tribological behavior of the FDs, mainly because of the different tribological mechanisms: in a FD two flat surfaces slide one on each other, while in a PoD test a cylindrical flat-ended indenter slides on a flat surface. Consequently, further experimental tests will be performed soon on the real device to evaluate the effectiveness of the scaled PoD tests in terms of reproduction of the tribological behavior of the FDs, and to estimate the real wear between the friction pads.

Author Contributions: Conceptualization, A.A. and M.Z.; methodology, E.G., E.B., A.F. and M.Z.; validation, E.G. and E.B.; formal analysis, E.G. and E.B.; investigation, E.G., E.B. and A.F.; resources, A.A., A.F. and M.M.; data curation, E.G.; writing—original draft preparation, E.G. and E.B.; writing—review and editing, A.A., A.F., M.Z. and M.M.; visualization, E.G. and E.B.; supervision, A.A. and M.M.; project administration, A.A.; funding acquisition, A.A. All authors have read and agreed to the published version of the manuscript.

Funding: This research was funded by FAR funding from the University of Ferrara (Ferrara, Italy), years 2020: "Bidirectional Friction Links for Seismic Retrofit of Existing Precast RC Structures" (Grant No. FAR2078914) and 2021: "A friction damper for seismic retrofit of precast RC structures" (Grant No. FAR2151302). This research was also funded by FIRD funding from the University of Ferrara (Ferrara, Italy), year 2022: "Mechanical and tribological testing of a novel damping device for seismic risk mitigation of industrial buildings" (Grant No. FIRD_DE_AA_001).

Institutional Review Board Statement: Not applicable.

Informed Consent Statement: Not applicable.

Data Availability Statement: Not applicable.

Acknowledgments: The authors acknowledge Eng. Michele Bandini by Peen Service S.r.l., Bologna, Italy, for carrying out the shot peening treatments. The authors also gratefully acknowledge Alberto Castellero and Paola Rizzi by the Department of Chemistry, Metallic Materials research group, University of Torino (Torino, Italy), for performing the nanoindentation tests. Finally, the authors acknowledge Michele Pinelli and Alessio Suman by the Department of Engineering, Fluid Machinery and Energy Systems research group, University of Ferrara (Ferrara, Italy), for performing the weight loss measurements.

Conflicts of Interest: The authors declare no conflict of interest.

Nomenclature

A	Wear track's area (mm^2)
COF_{st}	Mean COF value of the second steady-state stage
$COF_{st}{}'$	Mean COF value of the first steady-state stage
$cv_{COF,st}$	Coefficient of variation of the second steady-stage state defined as the ratio between the mean standard deviation and mean COF value
$cv_{COF,st}{}'$	Coefficient of variation of the first steady-stage state defined as the ratio between the mean standard deviation and mean COF value
d	Wear tracks depth (μm)
F	Applied load (N)
Ra	Superficial roughness (μm)
S	Wear track's length (mm)
S_{tot}	Total sliding length (m)
t	Treatment thickness (μm)
$t_{st}{}'$	Duration of the first steady-state stage (s)
t_{tr}	Transition time of the second steady-state stage (s)
$t_{tr}{}'$	Transition time of the first steady-state stage (s)
w	Wear tracks width (mm)
WR_d	Specific wear rate on the disk (mm^3/Nm)
WR_p	Specific wear rate on the pin (mm^3/Nm)
Δg	Pin's mass loss (g)
ΔV	Disk's volume loss (mm^3)
ρ	Pin's mass density (g/mm^3)
NI	Disk subjected to electrolytic nickel plating
SP1	Disk subjected to shot peening and Ra = 1 μm
SP2	Disk subjected to shot peening and Ra = 2 μm
TR	Original turned disk used as a reference
ZN	Disk subjected to zinc plating

References

1. Christopoulos, C.; Filatrault, A. *Principles of Passive Supplemental Damping and Seismic Isolation*; IUSS Press: Pavia, Italy, 2006; ISBN 978-88-7358-037-9.
2. Calvi, P.M.; Calvi, G.M. Historical Development of Friction-Based Seismic Isolation Systems. *Soil Dyn. Earthq. Eng.* **2018**, *106*, 14–30. [CrossRef]
3. Soong, T.T.; Spencer, B.F. Supplemental Energy Dissipation: State-of-the-Art and State-of-the-Practice. *Eng. Struct.* **2002**, *24*, 243–259. [CrossRef]
4. Latour, M.; Piluso, V.; Rizzano, G. Experimental Behaviour of Friction T-Stub Beam-to-Column Joints under Cyclic Loads. *Steel. Constr.* **2013**, *6*, 11–18. [CrossRef]
5. Khoo, H.H.; Clifton, C.; Butterworth, J.; Macrae, G. Experimental Study of Full-Scale Self-Centering Sliding Hinge Joint Connections with Friction Ring Springs. *J. Earthq. Eng.* **2013**, *17*, 972–997. [CrossRef]
6. Latour, M.; Piluso, V.; Rizzano, G. Experimental Analysis of Innovative Dissipative Bolted Double Split Tee Beam-to-Column Connections. *Steel. Constr.* **2011**, *4*, 53–64. [CrossRef]
7. Latour, M.; Piluso, V.; Rizzano, G. Free from Damage Beam-to-Column Joints: Testing and Design of DST Connections with Friction Pads. *Eng. Struct.* **2015**, *85*, 219–233. [CrossRef]
8. Grigorian, C.E.; Yang, T.S.; Popov, E.P. Slotted Bolted Connection Energy Dissipators. *Earthq. Spectra.* **1993**, *9*, 491–504. [CrossRef]
9. Hutchings, I.M.; Shipway, P. *Tribology: Friction and Wear of Engineering Materials*, 2nd ed.; Butterworth-Heinemann: Oxford, UK, 2017; ISBN 9780081009109.
10. Bhushan, B. *Introduction to Tribology*, 2ed ed.; John Wiley & Sons Inc.: Chichester, UK, 2013.
11. Liang, G.; Schmauder, S.; Lyu, M.; Schneider, Y.; Zhang, C.; Han, Y. An Investigation of the Influence of Initial Roughness on the Friction and Wear Behavior of Ground Surfaces. *Materials* **2018**, *11*, 237. [CrossRef] [PubMed]
12. Marder, A.; Goodwin, F. *The Metallurgy of Zinc Coated Steels*; Elsevier—Health Sciences Division: Amsterdam, The Netherlands, 2023.
13. Sriraman, K.R.; Manimunda, P.; Chromik, R.R.; Yue, S. Effect of Crystallographic Orientation on the Tribological Behavior of Electrodeposited Zn Coatings. *RSC Adv.* **2016**, *6*, 17360–17372. [CrossRef]
14. Sriraman, K.R.; Strauss, H.W.; Brahimi, S.; Chromik, R.R.; Szpunar, J.A.; Osborne, J.H.; Yue, S. Tribological Behavior of Electrodeposited Zn, Zn–Ni, Cd and Cd–Ti Coatings on Low Carbon Steel Substrates. *Tribol. Int.* **2012**, *56*, 107–120. [CrossRef]
15. Tafreshi, M.; Allahkaram, S.R.; Farhangi, H. Comparative Study on Structure, Corrosion Properties and Tribological Behavior of Pure Zn and Different Zn-Ni Alloy Coatings. *Mater. Chem. Phys.* **2016**, *183*, 263–272. [CrossRef]
16. Kawagoishi, N.; Nagano, T.; Moriyama, M.; Kondo, E. Improvement of Fatigue Strength of Maraging Steel by Shot Peening. *Mater. Manuf. Process.* **2009**, *24*, 1431–1435. [CrossRef]
17. Bagheri, S.; Guagliano, M. Review of Shot Peening Processes to Obtain Nanocrystalline Surfaces in Metal Alloys. *Surf. Eng.* **2009**, *25*, 3–14. [CrossRef]
18. Trung, P.Q.; Khun, N.W.; Butler, D.L. Effects of Shot Peening Pressure, Media Type and Double Shot Peening on the Microstructure, Mechanical and Tribological Properties of Low-Alloy Steel. *Surf. Topogr.* **2016**, *4*, 045001. [CrossRef]
19. Khun, N.W.; Trung, P.Q.; Butler, D.L. Mechanical and Tribological Properties of Shot-Peened SAE 1070 Steel. *Tribol. Trans.* **2016**, *59*, 932–943. [CrossRef]
20. Latour, M.; Piluso, V.; Rizzano, G. Experimental Analysis on Friction Materials for Supplemental Damping Devices. *Constr. Build. Mater.* **2014**, *65*, 159–176. [CrossRef]
21. Khoo, H.H.; Clifton, C.; Butterworth, J.; MacRae, G.; Ferguson, G. Influence of Steel Shim Hardness on the Sliding Hinge Joint Performance. *J. Constr. Steel. Res.* **2012**, *72*, 119–129. [CrossRef]
22. Mualla, I.H.; Belev, B. Performance of Steel Frames with a New Friction Damper Device under Earthquake Excitation. *Eng. Struct.* **2002**, *24*, 365–371. [CrossRef]
23. Sinha, A.; Ischia, G.; Menapace, C.; Gialanella, S. Experimental Characterization Protocols for Wear Products from Disc Brake Materials. *Atmosphere* **2020**, *11*, 1102. [CrossRef]
24. Chandra Verma, P.; Menapace, L.; Bonfanti, A.; Ciudin, R.; Gialanella, S.; Straffelini, G. Braking Pad-Disc System: Wear Mechanisms and Formation of Wear Fragments. *Wear* **2015**, *322–323*, 251–258. [CrossRef]
25. Straffelini, G.; Pellizzari, M.; Molinari, A. Influence of Load and Temperature on the Dry Sliding Behaviour of Al-Based Metal-Matrix-Composites against Friction Material. *Wear* **2004**, *256*, 754–763. [CrossRef]
26. Grossi, E.; Aprile, A.; Zerbin, M. Tribological Investigation on Metal Mating Surfaces to Explore Real Use Conditions of a Novel Friction Damper for Seismic Applications. *Eng. Struct.* **2023**, *278*, 115473. [CrossRef]
27. Vaxevanidis, N.M.; Manolakos, D.E.; Koutsomichalis, A.; Petropoulos, G.; Panagotas, A.; Sideris, I.; Mourlas, A.; Antoniou, S.S. The Effect of Shot Peening on Surface Integrity and Tribological Behaviour of Tool Steels. In Proceedings of the International Conference on Tribology, Parma, Italy, 20–22 September 2006.
28. *EN ISO 25178-2:2021*; CEN Geometrical Product Specifications (GPS)—Surface Texture: Areal—Part 2: Terms, Definitions and Surface Texture Parameters. International Organization for Standardization: Geneva, Switzerland, 2022.
29. *UNI EN ISO 21920-3:2021*; Geometrical Product Specifications (GPS)—Surface Texture: Profile—Part 3: Specification Operators. International Organization for Standardization: Geneva, Switzerland, 2021.

30. Wu, B.; Xu, B.-s.; Zhang, B.; Dong, S.-y. The Effects of Parameters on the Mechanical Properties of Ni-Based Coatings Prepared by Automatic Brush Plating Technology. *Surf. Coat. Technol.* **2007**, *201*, 5758–5765. [CrossRef]
31. *UNI EN ISO 14577-1*; Metallic Materials—Instrumented Indentation Test for Hardness and Materials Parameters—Part 1: Test Method. International Organization for Standardization: Geneva, Switzerland, 2015.
32. Blau, P.J. On the Nature of Running-In. *Tribol. Int.* **2005**, *38*, 1007–1012. [CrossRef]
33. Fereidouni, H.; Akbarzadeh, S.; Khonsari, M.M. The Relation Between Subsurface Stresses and Useful Wear Life in Sliding Contacts. *Tribol. Lett.* **2020**, *68*, 9. [CrossRef]